

Linear and nonlinear modeling and control of a power take-off simulation for wave energy conversion

C.J. Taylor¹, M.A. Stables¹, P. Cross¹, K. Gunn¹ and G.A. Aggidis¹

¹Engineering Department,
Lancaster University,
LA1 4YR, Lancaster, UK
E-mail: c.taylor@lancaster.ac.uk

Abstract

This article focuses on control of the power take off (PTO) element of a point absorber wave energy converter. The research is based on a nonlinear simulation of a PTO hydraulic circuit, in which the piston velocity and generator torque act as ‘disturbance’ and control actuator variables respectively, whilst the damping force is the controlled output variable. The piston velocity is generated by a hydrodynamic simulation model that reacts to both the damping force and sea wave profile. The damping force set point will be obtained from an associated power capture optimisation module and may be time varying. However, it is clear that such an adaptive tuning system also requires high performance ‘low-level’ control of the device actuators, in order to fully realise the benefits of optimisation. In this regard, the present article illustrates use of the Proportional-Integral-Plus (PIP) control methodology as applied to the PTO simulation. In their simplest linear form, such PIP controllers do not account for the interconnected system variables mentioned above. For this reason, the research also considers ‘feed-forward’ and ‘state-dependent’ forms of PIP control, in which the piston velocity is appended to a non-minimal state space representation of the system.

Keywords: SUPERGEN, power take off simulation, optimal control, non-minimal state space

Nomenclature

k_l	= motor leakage co-efficient
v	= piston velocity
A	= pipe cross-sectional area
B	= friction coefficient
D	= motor constant
D_h	= hydraulic diameter of pipe
y	= damping force
K_S	= pipe cross-section shape factor
L	= motor shaft angular momentum
L_g	= geometrical length of pipe

L_{eq}	= equivalent length of local resistances
J	= moment of inertia
P_{pr}	= accumulator pre-charge pressure
Re	= Reynolds number
S	= piston cylinder cross-section area
u	= torque applied to motor shaft
V	= volume of oil in accumulator
V_A	= volume of accumulator
η_m	= motor efficiency
κ	= specific heat ratio
ρ	= density of oil

Subscripts

k	= value at k th sample
-----	--------------------------

Superscripts

\cdot	= first derivative
---------	--------------------

1 Introduction

One of the most challenging problems in the development of wave energy converters (WECs) relates to their optimisation and control in order to maximise energy conversion. In order to extract the maximum amount of energy from ocean waves, the resonant frequency of a WEC should match the dominant frequency of the wave spectrum as it changes with variations in sea state. In general, it is possible to adjust the resistance of the device to movement caused by the action of waves and thereby tune the WEC to this frequency. In the present article, this is achieved by changing the damping force in the power take off (PTO) mechanism.

Many WEC control strategies have been proposed including, for example, latching [1] and various adaptive tuning methods [2, 3]. In order to evaluate and implement such control strategies, they have to be optimised for realistic sea states. This optimisation process can be arduous and must be repeated if the system state changes; for example, if predictions of future waves are made available to the control system.

Recent research at Lancaster has focused on the development of generic strategies for WEC optimisation based on the use of Evolutionary Algorithms (EAs). In particular, reference [4] utilises a real coded EA and a novel time domain model of a point absorber WEC [3] to optimise power capture. One advantage of EAs in this context, is their potential extension to machine learning. In this case, an initial model-based optimisation step would be followed by application to the real device, allowing the controller to continue to develop on-line.

However, it is clear that such an adaptive tuning module also requires high performance ‘low-level’ control of the device actuators. In other words, fast and accurate feedback control of nonlinear actuators is necessary in order to fully realise the benefits of the optimisation phase. To help investigate these issues, the present research couples a time domain WEC model (section 3) to an illustrative nonlinear simulation of a PTO hydraulic circuit (section 4).

Fig. 1 illustrates the connection between these models and the key variables considered in the article. Here, the piston velocity v_k and generator torque u_k represent disturbance and control input variables respectively, whilst the damping force y_k is regarded as the controlled output variable [5]. In fact, the damping force set point d_k is ultimately obtained from the optimisation module and may be time varying. Finally, the piston velocity is generated by the hydrodynamic model that is in turn driven by the damping force and an externally specified (and potentially nonlinear) sea wave profile.

In the present article, statistically obtained transfer function models are identified and used to design Proportional-Integral-Plus (PIP) control systems [6–11]. These are straightforward to implement and provide a logical extension of conventional PID controllers, with additional dynamic feedback compensators introduced automatically when the process is of greater than first order as here (section 5).

To illustrate the approach in the present context, a PIP controller is developed for the PTO element of the simulation (section 6). However, in their simplest linear form, such PIP controllers do not account for the interconnected system variables shown in Fig. 1 and this may lead to poor control performance for realistic nonlinear sea states. For this reason, two extended approaches to the design problem are suggested, based on feed-forward (section 6) and state dependent parameter (section 7) methods.

2 SUPERGEN

The research reported in this article takes place under the auspices of the Supergen Marine Energy Research Consortium. The over-arching objective of Phase 2 (2007-2011) of the project is to ‘Increase knowledge and understanding of the device-sea interactions of energy converters from model-scale in the laboratory to full size in the open sea’ (www.supergen-marine.org.uk). There are ten research workstreams led by 11 academic

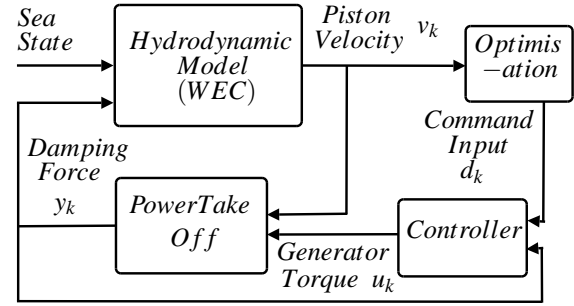


Figure 1: Schematic diagram of the WEC controller.

staff investigators across five core universities, including The University of Edinburgh, Heriot-Watt University, The University of Strathclyde, Lancaster University and Queens University Belfast.

Work stream 7 on advanced control and network integration started October 2008, with the aim to develop continuously adapting control techniques to optimise the energy extraction and survivability (of generic WECs). The objective of this work is to ensure that the effects of nonlinearity and non-stationarity of the marine resource on wave and tidal current energy conversion are well understood and satisfactorily mitigated through advanced, evolving and coordinated control of the devices and their power take-off system.

3 Optimisation

To evaluate dynamic (time varying) control systems in real seas, a time domain model of the WEC is required. Although evolutionary algorithms are known to be an efficient method for optimising within an extensive search space, a large number of evaluations of the model are necessary. For this reason, a recently developed computationally efficient WEC model is selected for the research and briefly reviewed below.

3.1 Hydrodynamic model

The model is based on the equations of motion of a simple mass–spring–damper system, initially considered in the frequency domain [3]. The coefficients of the equation represent the effect of water on the device, as shown below:

$$\{-\omega^2[\mathbf{M} + \mathbf{A}_\omega] + \mathbf{i}\omega\mathbf{B}_\omega + \mathbf{C}\}\xi_\omega = \mathbf{F}_\omega \quad (1)$$

ω is the angular frequency of the incoming waves (rad/s);

\mathbf{M} is the dry mass of the device (kg);

\mathbf{A}_ω is the ‘‘added mass’’ (kg);

\mathbf{B}_ω is the radiation damping (Nsm^{-1});

\mathbf{C} is the hydrodynamic stiffness or centralising force (Nm^{-1});

\mathbf{F}_ω is the wave excitation force (N); and

ξ is the complex displacement amplitude (m).

Here, the ‘added mass’ refers to the mass of water that moves with the device. Radiation damping is the energy lost in waves radiating from a moving object in still water. Hydrodynamic spring force refers to the buoyancy of a floating device, whilst the wave force is the force exerted by a wave on a stationary object. The hydrodynamic coefficients are derived by WAMIT, a computational fluid dynamics package developed at the Massachusetts Institute of Technology (www.wamit.com). WAMIT uses panel methods and potential flow theory to calculate the response of offshore structures to linear monochromatic waves. The model is subsequently converted into the time domain by fitting transfer functions to the three hydrodynamic forces. More detailed explanations of the complete model are given by [3].

In an extension to the basic formulation, the equations are updated to allow for time variation (hence optimisation and control) of the following three forces:

- Applied damping: the damping force applied by the PTO system.
- Applied stiffness: an additional applied spring force used to tune the device.
- Latching: an extreme damping force that can be applied or removed by the control system.

However, for the preliminary results reported in sections 4 through to 7, the last two forces above are ignored, i.e. only the PTO element is used for feedback control purposes.

3.2 Power capture optimisation

The ‘high level’ control problem is to optimise the external spring force and damping force required for maximum power capture. In this regard, the power carried by waves is usually represented as power per unit wave crest. The capture width of a device can, therefore, be conveniently represented as the length of wave crest captured in the current sea state. To convert this figure into a non-dimensional value, it is subsequently divided by the width of the device. In other words, a device with a capture width ratio of unity captures all of the energy that acts directly on it.

Reference [4] develops a generic approach for WEC optimisation using EAs. Simulation results are presented for tuning an illustrative device in both sinusoidal and Pierson Moskowitz [12] spectra waves; and for optimisation of both ‘slow tuning’ [2] and ‘latching’ [1] control systems. The EA is able to find optima for all the problems presented, despite the very large search domain required for the latching control problem. In fact, the proposed GA successfully optimises these control algorithms for realistic seas without prior assumptions. However, further work is required to refine the GA, in order to improve the robustness of the search and this is the focus of current research by the authors [4].

4 PTO simulation

Bacelli *et al* [5] derive a model of a hydraulic PTO for a point absorbing WEC, based on the schematic diagram shown in Fig. 2. In this model, a hydraulic piston connected to the oscillating body of the WEC produces an alternating flow of oil. Four non-return valves and a gas accumulator rectify and smooth the flow, whilst a hydraulic motor converts the flow into rotational momentum. The model also takes account of losses in the system, due to the drop in pressure along pipes, leakages and motor friction.

The velocity of the piston v and the applied torque on the shaft of the hydraulic motor u , are related to the damping force y by the means of five key equations. Two nonlinear state equations (2) describe the relationship between the volume of oil in the accumulator V , and the hydraulic motor shaft angular momentum L ,

$$\begin{aligned}\dot{V} &= -k_l \cdot h(V) - \frac{D}{J} \cdot L + S \cdot v \\ \dot{L} &= D\eta_m \cdot h(V) - \frac{B}{J} \cdot L - u\end{aligned}\quad (2)$$

where k_l , D , J , S , η_m and B are constant coefficients representing the motor leakage, motor constant, moment of inertia, the piston cylinder cross-sectional area, motor efficiency and friction respectively. An associated output equation relates the damping force to the oil volume and piston velocity, as follows,

$$y = S \cdot h(V) + S \cdot k(S \cdot v) \quad (3)$$

where $h(V)$ is the accumulator pressure,

$$h(V) = \frac{P_{pr}}{\left(1 - \frac{V}{V_A}\right)^\kappa} \quad (4)$$

and $k(S \cdot v)$ is the Haaland approximation of the Darcy equation for pressure loss due to friction, for laminar flow in a pipe, defined as follows,

$$k(S \cdot v) = \frac{K_S (L_g + L_{eq})}{\text{Re}} \frac{\rho}{D_h} \frac{S \cdot v}{2A^2} |S \cdot v| \quad (5)$$

In these equations, P_{pr} , V_A , κ , K_S , Re , L_g , L_{eq} , D_h , ρ and A are the accumulator pre-charge pressure, volume of accumulator, specific heat ratio, pipe cross-section shape factor, Reynolds number, geometrical length of the pipe, equivalent length of local resistances, hydraulic diameter of the pipe, density of oil and the pipe cross-sectional area respectively (all constant coefficients).

The PTO model is designed to work in tandem with a hydrodynamic model providing the data for piston velocity using the values for the damping force and sea state in a feedback loop, as illustrated in Fig. 1. However, for the preliminary research reported in the present article, the PTO model is considered in isolation, with the velocity of the piston defined as an external disturbance.

The state and output equations form the basis of a nonlinear Matlab/Simulink model of the PTO. Several

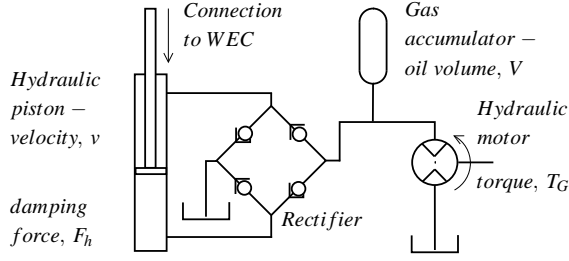


Figure 2: PTO hydraulic circuit (after [5])

Parameter	Value
S	0.1m^2
η_m	0.9
J	$7.6 \times 10^{-3}\text{kg/m}^2$
D	$1.88 \times 10^{-4}\text{m}^3$
B	0.1Nms
P_{pr}	$2 \times 10^6\text{Pa}$
κ	1.4
V_A	0.1m^3
k_l	$2.6 \times 10^{-11}\text{m}^5/\text{Ns}$
K_S	64
Re	2000
L_g	5m
L_{eq}	1m
D_h	0.04m
ρ	844kg/m^3
A	calculated from D_h

Table 1: PTO model parameters.

parameters for this model correspond to a commercially available fixed displacement hydraulic motor from the ‘Staffa’ range built by Kawasaki [13]. Although this motor is small in comparison to those present in full-size WECs, it is representative of a scaled-down model, such as those used for small-scale sea trials. Other parameters have been suggested by [5], several of which are initially based upon default values for the SimHydraulics extension to Simulink. The parameter values used in the present article are shown in Table 1.

5 Control methodology

For many nonlinear systems, the essential small perturbation behaviour can be very well approximated by simple linearised transfer function models and, to date, this has been the approach most commonly employed in PIP control system design [6, 8]. Such linear PIP control systems have been successfully employed in a wide range of practical applications; for example, to maintain verticality of a hydraulically operated vibro-lance used for foundation work on building sites [10].

However, to improve PIP control of nonlinear systems, recent research has instead utilised a quasi-linear State Dependent Parameter (SDP) model structure [14], in which the parameters are functionally dependent on other variables in the system. This formulation may then be used to design a SDP/PIP control law at each sam-

pling instant using linear methods, such as pole assignment [11] or suboptimal linear quadratic [9] design. The nonlinear approach is briefly reviewed below, whilst the linear case follows straightforwardly by using time invariant coefficients (see section 6 for an example).

5.1 System identification

Numerous publications describe an approach for the identification of SDP models; see e.g. [14, 15] and the references therein. The approach exploits recursive Kalman Filtering and Fixed Interval Smoothing (FIS) methods, within an iterative ‘backfitting’ algorithm that involves special re-ordering of the time series data. Consider the following SDP model in deterministic form,

$$y_k = \mathbf{w}_k^T \mathbf{p}_k \quad (6)$$

where,

$$\mathbf{w}_k^T = [-y_{k-1} \quad \cdots \quad -y_{k-n} \quad u_{k-1} \quad \cdots \quad u_{k-m}]$$

$$\mathbf{p}_k = [\mathbf{p}_{1,k} \quad \mathbf{p}_{2,k}]^T$$

$$\mathbf{p}_{1,k} = [a_1 \{ \chi_k \} \quad \cdots \quad a_n \{ \chi_k \}]$$

$$\mathbf{p}_{2,k} = [b_1 \{ \chi_k \} \quad \cdots \quad b_m \{ \chi_k \}]$$

Here y_k and u_k are the output and input variables respectively, while $a_i \{ \chi_k \}$ ($i = 1, 2, \dots, n$) and $b_j \{ \chi_k \}$ ($j = 1, \dots, m$) are state dependent parameters. The latter are assumed to be functions of a non-minimal state vector χ_k^T . For SDP/PIP control system design, it is usually sufficient to limit the model (6) to the case that $\chi_k^T = \mathbf{w}_k^T$. Finally, any pure time delay is represented by setting the leading $b_j \{ \chi_k \}$ terms to zero.

The first stage of the analysis involves the identification of conventional linear models, for which $a_i \{ \chi_k \} = a_i$ and $b_j \{ \chi_k \} = b_j$ are time invariant. This helps to define the initial structure of the SDP model above. In this case, equation (6) is usually represented in the form of a discrete-time transfer function and the present research uses an optimal refined instrumental variable algorithm to estimate the parameters [15]. The two main statistical measures utilised to help identify the most appropriate model structure, are the coefficient of determination R_7^2 , based on the response error; and Young’s Identification Criterion (YIC), which provides a combined measure of model fit and parametric efficiency.

5.2 Control design

The non-minimal state space representation of the system (6) is,

$$\begin{aligned} \mathbf{x}_{k+1} &= \mathbf{F} \{ \chi_{k+1} \} \mathbf{x}_k + \mathbf{g} \{ \chi_{k+1} \} u_k + \mathbf{d}r_{k+1} \\ y_k &= \mathbf{h} \mathbf{x}_k \end{aligned} \quad (7)$$

where the $n + m$ non-minimal state vector is,

$$\mathbf{x}_k = [y_k \quad \cdots \quad y_{k-n+1} \quad u_{k-1} \quad \cdots \quad u_{k-m+1} \quad z_k]^T \quad (8)$$

and $z_k = z_{k-1} + [d_k - y_k]$ is the integral-of-error between the reference or command input d_k and the sampled output y_k . Inherent type 1 servomechanism performance is

introduced by means of this integral-of-error state. For brevity, the $\mathbf{F}\{\chi_k\}$, $\mathbf{g}\{\chi_k\}$, \mathbf{d} and \mathbf{h} definitions are omitted: see [9] for details. Finally, the PIP control law takes the following state variable feedback form,

$$u_k = -\mathbf{c}\{\chi_k\} \mathbf{x}_k \quad (9)$$

where the state dependent control gain vector,

$$\mathbf{c}\{\chi_k\} = [f_{0,k}, \dots, f_{n-1,k}, g_{1,k}, \dots, g_{m-1,k}, -k_{I,k}] \quad (10)$$

is obtained by either pole assignment [11] or optimisation of a linear quadratic cost function using a state dependent Riccati equation [9]. In either case, Fig. 3 illustrates the controller in block diagram form, where,

$$\begin{aligned} F_1\{\chi_k, z^{-1}\} &= f_{1,k}z^{-1} + \dots + f_{n-1,k}z^{-n+1} \\ G\{\chi_k, z^{-1}\} &= 1 + g_{1,k}z^{-1} + \dots + g_{m-1,k}z^{-m+1} \end{aligned}$$

while $f_{0,k}$ and $k_{I,k}$ are the time varying (state dependent) proportional and integral gains respectively. Finally, $A\{\chi_k, z^{-1}\}$ and $B\{\chi_k, z^{-1}\}$ are polynomials in the backward shift operator ($z^{-1}y_k = y_{k-1}$), i.e. the pseudo-transfer function representation the SDP model (6).

In the linear case, these approaches reduce to the standard time invariant form [6, 8]. The required stability and pole assignability (or controllability in the linear case) results are omitted here for brevity but are developed by the earlier publications cited above.

6 Worked example – linear control

As discussed above, a ‘low-level’ PIP control strategy is required to ensure the PTO reaches a desired value for the damping force, where the latter is set by the ‘high-level’ controller in order to optimise the response of the WEC to the current sea state. In the present worked example, however, the damping force set point has been arbitrarily chosen to illustrate the ‘low-level’ approach. Furthermore, the example focuses on linear (time invariant) PIP design, whilst potential improvements using the nonlinear approach are considered in section 7.

For linear PIP design, equation (6) may be represented in conventional transfer function form,

$$y_k = \frac{B(z^{-1})}{A(z^{-1})} u_k \quad (11)$$

Here, y_k and u_k are the sampled damping force (output) and generator torque (control input) variables respectively, whilst $B(z^{-1})$ and $A(z^{-1})$ are polynomials in the backward shift operator, i.e. $B(z^{-1}) = b_1z^{-1} + b_2z^{-2} + \dots + b_mz^{-m}$ and $A(z^{-1}) = 1 + a_1z^{-1} + \dots + a_nz^{-n}$.

6.1 Linear model identification

Equation (11) is identified using data obtained by perturbing the open-loop simulation about an equilibrium point. For the present example, the following second order transfer function with unity time delay, yields a good representation of the system suitable for linear PIP

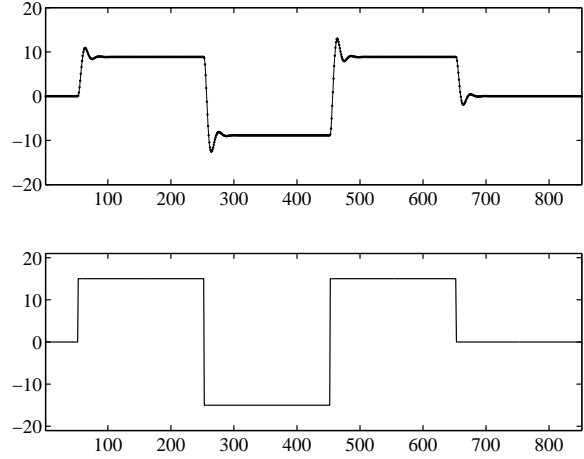


Figure 4: Linear model response compared to PTO simulation for small perturbations close to an operating point, with the baseline removed in the graphs. Upper subplot: simulated damping force (dots) and linear model fit (solid), plotted against sample number. Lower subplot: motor torque.

design, with $R_T^2 = 0.9999$ and $YIC = -22.649$ respectively,

$$y_k = \frac{b_1z^{-1}}{1 + a_1z^{-1} + a_2z^{-2}} u_k \quad (12)$$

To obtain the control model (12), simulated data are collected at a sampling rate of 0.02 seconds. Experimentation suggests that such a sampling rate allows for the estimation of a suitable backward shift operator model and is fast enough to handle the disturbances associated with the piston velocity. Fig. 4 illustrates the model fit with the chosen equilibrium levels removed. Here, the upper and lower subplots show y_k and u_k respectively, with the response of the nonlinear PTO simulation and equation (12) visually indistinguishable.

6.2 Linear control design

Equation (12) is represented in non-minimal state space form (7) as follows, where $\mathbf{F}\{\chi_k\} = \mathbf{F}$ and $\mathbf{g}\{\chi_k\} = \mathbf{g}$ are again time invariant in this linear case,

$$\begin{bmatrix} y_k \\ y_{k-1} \\ z_k \end{bmatrix} = \begin{bmatrix} -a_1 & -a_2 & 0 \\ 1 & 0 & 0 \\ a_1 & a_2 & 1 \end{bmatrix} \begin{bmatrix} y_{k-1} \\ y_{k-2} \\ z_{k-1} \end{bmatrix} + \begin{bmatrix} b_1 \\ 0 \\ -b_1 \end{bmatrix} u_{k-1} + \begin{bmatrix} 0 \\ 0 \\ 1 \end{bmatrix} r_k \quad (13)$$

$$y_k = [1 \ 0 \ 0] \begin{bmatrix} y_k \\ y_{k-1} \\ z_k \end{bmatrix} \quad (14)$$

The PIP control law (9) is,

$$u_k = - [f_0 \ f_1 \ -k_I] \begin{bmatrix} y_k \\ y_{k-1} \\ z_k \end{bmatrix} \quad (15)$$

where f_0 and k_I are the proportional and integral gains respectively, whilst f_1 is an additional feedback gain required for PIP control of the model (12). There are no

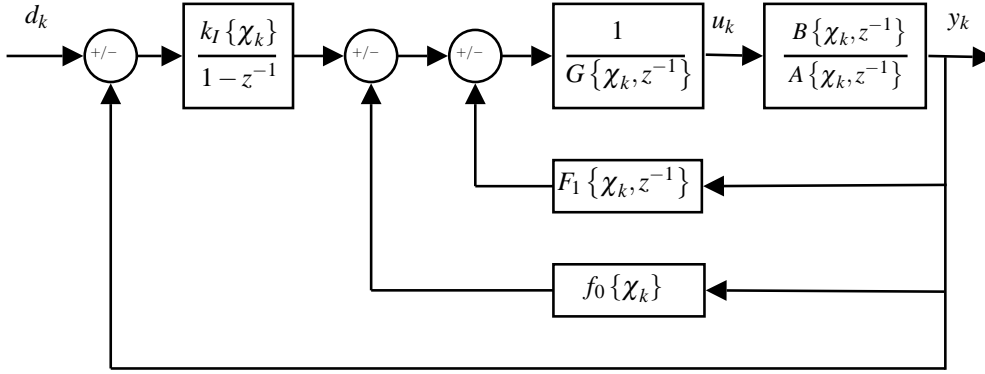


Figure 3: Proportional-Integral-Plus (PIP) control structure.

input compensators in this case, since the system has a time delay of one sampling interval and the transfer function has no zeros. Furthermore, for linear PIP design, the gain vector (10) is time invariant, i.e. $\mathbf{c}\{\chi_k\} = \mathbf{c}$.

The control gains are conveniently obtained by minimising the following standard linear quadratic cost function,

$$J = \frac{1}{2} \sum_{i=0}^{\infty} \mathbf{x}_i^T \mathbf{Q} \mathbf{x}_i + r u_i^2 \quad (16)$$

where r is a positive scalar and \mathbf{Q} is a symmetric, positive semi-definite matrix, the diagonal elements of which define the weights associated with current and past values of the output, past values of the input (when these exist as state variables) and the integral-of-error state. For the present example, satisfactory closed-loop performance is obtained by setting $\mathbf{Q} = \text{diag}[1 \ 100 \ 0.5]$ and $r = 1$. Solution of the ubiquitous Riccati equation yields $\mathbf{c} = [13.9536 \ -8.3973 \ 0.4606]$.

This single-input, single-output PIP controller may be implemented in two ways: (i) the standard feedback form, which is similar in structure to a conventional PI controller or (ii) in a forward-path form in which the inner loop of the controller is eliminated to form a single forward-path transfer function (or pre-compensation filter). Each of these has advantages in practice [7] and so both implementations are examined here.

When the above PIP algorithm is applied to the full nonlinear PTO simulation with no disturbances (i.e. the piston velocity is unrealistically fixed constant), Fig. 5 shows that the two control structures yield very similar results. However, once the piston velocity is included as a sinusoidal disturbance signal, the feedback form is found to yield considerably improved performance over the forward-path form, as shown in Fig. 6.

To investigate further improvements in the disturbance rejection properties of the controller, several novel multiple-input ‘feedforward’ forms of PIP control are presently being investigated by the authors, and these results will be reported in future publications. Here, the piston velocity is considered as an additional measured or estimated state variable. In contrast to the above approach, multiple-input, single-output transfer function models are obtained from the nonlinear PTO simulation. These models represent the relationship between

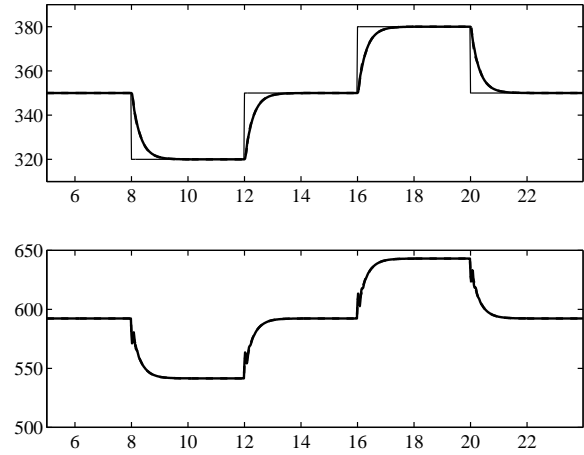


Figure 5: Closed-loop response with no disturbance. Upper subplot: command input (sequence of steps) and damping force, where the feedback and forward path structures yield visually indistinguishable responses, plotted against time (seconds). Lower subplot: generator torque.

the damping force output and both the hydraulic motor torque and piston velocity as input variables. In fact, preliminary results using this approach and based on an explicit model-based cancellation of the disturbance are illustrated in Fig. 7. Here, the new feedforward approach yields an improvement over the standard PIP structure discussed above, for the particular simulation experiment shown.

7 State-dependent models

In order to sufficiently excite the nonlinear dynamics of the PTO simulation for SDP modelling purposes, the open-loop generator torque and piston velocity are represented by independent Pseudo-Random Binary Signals (PRBS). In each case, the level and duration of the changing input signal is determined from a Gaussian distribution across the likely operating range of the system, as illustrated in Fig. 8. In contrast to Fig. 4, the PTO system is no longer limited to one operating level, hence the linear model response given by equation (12) is relatively poor, as illustrated by the thin trace in Fig. 8. However, a multiple-input (u_k, v_k), single output (y_k) SDP model yields a good model fit ($R_7^2=0.9$). The new model

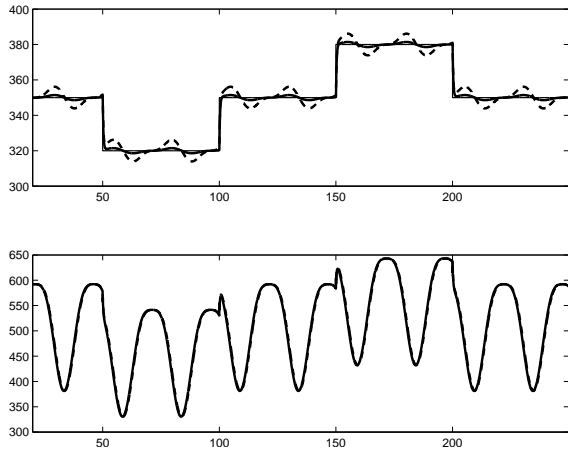


Figure 6: Closed-loop response with piston velocity disturbance represented as a sine wave. Upper subplot: command input (sequence of steps) and damping force controlled using the feedback (solid) and forward path (dashed) PIP structures, plotted against time (seconds). Lower subplot: generator torque.

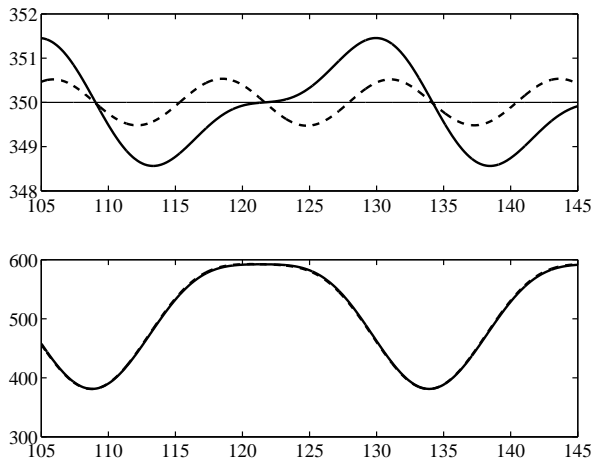


Figure 7: Closed-loop response with piston velocity disturbance represented as a sine wave. Upper subplot: command input (constant) and damping force controlled using the single-input (solid) and multiple-input feedforward (dashed) PIP structures, plotted against time (seconds). Lower subplot: generator torque.

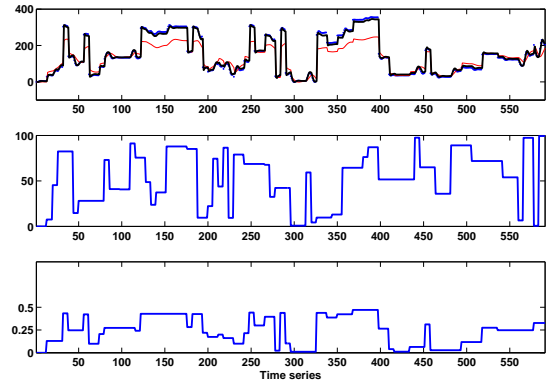


Figure 8: Linear and SDP model fit for a range of operating levels. Upper subplot: PTO simulation response (dots), SDP model (thick trace) and linear model (thin), plotted against sample number. Middle: generator torque. Lower: piston velocity.

is based on equation (6) with,

$$\begin{aligned} \mathbf{w}_k^T &= [-y_{k-1} \quad -y_{k-2} \quad u_{k-1} \quad v_{k-1} \quad v_{k-2} \quad v_{k-3}] \\ \mathbf{p}_{1,k} &= [a_1 \{\mathcal{X}_k\} \quad a_2 \{\mathcal{X}_k\} \quad b_1 \{\mathcal{X}_k\}] \\ \mathbf{p}_{2,k} &= [c_1 \{\mathcal{X}_k\} \quad c_2 \{\mathcal{X}_k\} \quad c_3 \{\mathcal{X}_k\}] \end{aligned} \quad (17)$$

The state dependent parameters are illustrated in Fig. 9, in which the parameters are found to be linear functions of the states in \mathbf{w}_k^T . The SDP/PIP control system associated with equation (17) is presently being developed. Hence, the relative performance and robustness of the new controller, applied to the full WEC simulation in Fig. 1 is the subject of ongoing research by the authors. However, the improved fit of the nonlinear model, illustrated in Fig. 8, presages a likely improvement in the associated controller performance, particularly in response to large piston velocity disturbances. Such large disturbances would take the damping force relatively far from the operating level used by the linear controller.

8 Conclusions

This article has illustrated the application of proportional-integral-plus (PIP) control methods to a nonlinear power take off (PTO) hydraulic circuit simulation model. Here, the generator torque is used to regulate the applied damping force of the wave energy converter. Although the damping force set point will ultimately be obtained from a power capture optimisation module also being developed by the authors [4], the present article has focused on the low level PIP control problem.

Linear transfer function models provide a good description of PTO behaviour, suitable for control system design close to a specified operating level. Although basic PIP design using single-input, single-output models yields reasonably good performance and robustness, this approach does not fully account for the nonlinearities in the system.

In order to improve the results, therefore, the article suggests and briefly evaluates feedforward and state

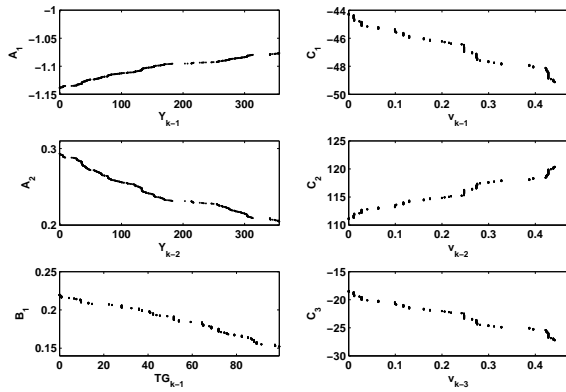


Figure 9: SDP model parameters associated with Fig. 8. The left hand side subplots show the state dependent parameters $a_1 \{\chi_k\}$, $a_2 \{\chi_k\}$ and $b_1 \{\chi_k\}$ (from top to bottom) plotted against delayed generator torque, whilst the right hand side subplots show $c_1 \{\chi_k\}$, $c_2 \{\chi_k\}$ and $c_3 \{\chi_k\}$ plotted against delayed piston velocity.

dependent forms of PIP control. Here, the piston velocity is appended to a non-minimal state space representation of the system to better represent the interconnections between the coupled PTO and hydrodynamic models. Clearly the next stage of the research is further develop and evaluate these approaches for a range of sea states. Furthermore, the coupled hydrodynamic PTO simulation model should be evaluated against experimental data since the present results have been limited to these physically-based models.

Acknowledgements

The authors are grateful for the support of the EP-SRC, colleagues in the Supergen Marine Energy Research Consortium and to the authors of reference [5]. The modelling and control tools have been assembled as the CAPTAIN toolbox [15] within the Matlab® software environment and may be downloaded from: www.es.lancs.ac.uk/cres/captain.

References

[1] A. Babarit and A. H. Clément. Optimal latching control of a wave energy device in regular and irregular waves. *Applied Ocean Research*, 28(2):77–91, 2006.

[2] D. J. Pizer. Maximum wave-power absorption of point absorbers under motion constraints. *Applied Ocean Research*, 15(4):227–234, 1993.

[3] H. Yavuz, T. J. Stallard, A. P. McCabe, and G. A. Aggidis. Time series analysis-based adaptive tuning techniques for a heaving wave energy converter in irregular

seas. *IMECHE Proceedings Part A Journal of Power and Energy*, 221:77–90, 2007.

- [4] K. Gunn and C. J. Taylor. Evolutionary algorithms for the development and optimisation of wave energy converter control systems. Submitted to *8th European Wave and Tidal Energy Conference*, Uppsala, Sweden, September, 2009.
- [5] G. Bacelli, J. C. Gilloteaux, and J. Ringwood. State space model of a hydraulic power take off unit for wave energy conversion using bondgraphs. In *Proceedings World Renewable Energy Conference*, Glasgow, UK, 2008.
- [6] P. C. Young, M. A. Behzadi, C. L. Wang, and A. Chotai. Direct digital and adaptive control by input-output, state variable feedback pole assignment. *International Journal of Control*, 46:1867–1881, 1987.
- [7] C. J. Taylor, A. Chotai, and P. C. Young. Proportional-Integral-Plus (PIP) control of time delay systems. *IMECHE Proceedings Part I Journal of Systems and Control Engineering*, 212:37–48, 1998.
- [8] C. J. Taylor, A. Chotai, and P. C. Young. State space control system design based on non-minimal state-variable feedback: Further generalisation and unification results. *International Journal of Control*, 73:1329–1345, 2000.
- [9] C. J. Taylor, E. M. Shaban, M. A. Stables, and S. Ako. Proportional-Integral-Plus (PIP) control applications of state dependent parameter models. *IMECHE Proceedings Part I Journal of Systems and Control Engineering*, 221(17):1019–1032, 2007.
- [10] E. M. Shaban, S. Ako, C. J. Taylor, and D. W. Seward. Development of an automated verticality alignment system for a vibro-lance. *Automation in Construction*, 17:645–655, 2008.
- [11] C. J. Taylor, A. Chotai, and P. C. Young. Non-linear control by input-output state variable feedback pole assignment. *International Journal of Control*, doi:10.1080/00207170802400970 (In Press), 2009.
- [12] W. H. Michel. Sea spectra revisited. *Marine Technology*, 36(4):211–227, 1999.
- [13] Kawasaki Precision Machinery. *Staffa Fixed Displacement Hydraulic Motor*, 2005.
- [14] P. C. Young, P. McKenna, and J. Bruun. Identification of nonlinear stochastic systems by state dependent parameter estimation. *International Journal of Control*, 74:1837–1857, 2001.
- [15] C. J. Taylor, D. J. Pedregal, P. C. Young, and W. Tych. Environmental time series analysis and forecasting with the Captain Toolbox. *Environmental Modelling and Software*, 22(6):797–814, 2007.